A Constitutive Model for Jointed Rock Mass

A. Azami[1], T. Yacoub[1], J. Curran[1,2] & D. Wai[1]
[1] *Rocscience Inc., Toronto, Ontario, Canada*
[2] *Civil Engineering, University of Toronto, Canada*

ABSTRACT: The effects of strength anisotropy of rock masses in slope stability problems are the focus of this paper. The source of the strength anisotropy can be attributed to many factors and the motivation of this study is to concentrate on the effects of planes of weakness, such as joints and bedding planes on the slope stability analysis. The limit equilibrium approach and finite element with shear strength reduction method are used for numerical simulations of slope stability problems. The finite element simulations take advantage of a constitutive model with embedded weak planes. The results obtained from the two methods are compared with each other.

1 INTRODUCTION

Natural soils and sedimentary rocks, such as shale, limestone and mudstone, are typically formed by deposition and progressive consolidation during formation. Such formations usually have a distinct internal structure, which is characterized by the appearance of multiple sedimentary layers. Besides the bedding planes, the geometric layout of networks of joints and other types of discontinuities in a rock mass are significant contributors to the complex behavior of such geomaterials (e.g. Hoek & Brown 1980, Hoek 1983, Zienkiewicz & Pande 1977). The presence of these fissures and planes of weakness significantly influence the response of geotechnical structures such as slopes, tunnels and excavations (Goodman et al, 1968, Bandis et al, 1983).

2 JOINTED ROCK MASS

The jointed rock mass here is considered to be composed of an intact material that is intercepted by up to three sets of weak planes. The spacing of the weak planes is such that the overall effects of the sets can be smeared and averaged over the control volume of the material. Such a configuration with two sets of weak planes is illustrated in Figure 1 where the weak planes are oriented at an arbitrary angle θ_1 and θ_2 in the rock mass.

In this paper, it is assumed that the failure of the matrix can be described by the Generalized Hoek-Brown criterion presented in Equation 1. The strength criterion of the weak planes is formulated by a simple Coulomb criterion as in Equation 2.

$$\sigma_1 - \sigma_3 - \sigma_{ci}\left(m_b \frac{\sigma_3}{\sigma_{ci}} + s\right)^a = 0 \tag{1}$$

$$\tau = \sigma_n \tan\varphi + c \tag{2}$$

In the above, σ_1 and σ_3 are the major and minor principal stresses, σ_{ci} is the uniaxial compressive strength of the intact rock material, and

$$m_b = m_i \exp\left(\frac{GSI - 100}{28 - 14D}\right) \tag{3a}$$

$$s = \exp\left(\frac{GSI - 100}{9 - 3D}\right) \tag{3b}$$

$$a = \frac{1}{2} + \frac{1}{6}\left[\exp\left(\frac{GSI}{15}\right) - \exp\left(\frac{-20}{3}\right)\right] \tag{3c}$$

m_i is an intact rock material property, GSI is the geological strength index, and D is the disturbance factor (Hoek et al 2002). τ and σ_n are the tangential and normal components of the traction vector on a weak plane, φ is the friction angle and c is the cohesion of the weak plane.

According to Equation 3, the strength of the rock mass is related to the strength of the intact rock that is factored by GSI and D parameters. In general, the presence of weak planes contributes to these two factors. In this work however, since the weak planes are considered in the modeling separately, the GSI and D parameters are selected to be very close to that of the intact rock. This will help capture the anisotropic effects caused by dominant weak planes in a rock mass.

3 CONSTITUTIVE MODEL

The constitutive model developed for the commercial finite element package, *Phase*[2] (Rocscience Inc. 2011), considers the Generalized Hoek-Brown model for the matrix and can include up to three sets of Coulomb weak planes. Tension cut offs are also considered for the matrix and the weak planes. In the formulation of this constitutive model, the total number of yield functions adds up to eight, not all of which needs to be active simultaneously. In the following sections the integration procedure of the constitutive equations and some application examples are presented.

3.1 *Integration of the constitutive equations*

Considering a multi-yield surface constitutive model where $F_\alpha(\sigma_{ij}) = 0$ is a set of yield surfaces and $Q_\alpha(\sigma_{ij}) = const.$, the corresponding set of plastic potentials, the basic elasto-plastic equations are:

$$\dot{\varepsilon}_{ij} = \dot{\varepsilon}_{ij}^{e} + \dot{\varepsilon}_{ij}^{p} \tag{4a}$$

$$\dot{\sigma}_{ij} = D_{ijkl}^{e} \dot{\varepsilon}_{kl}^{e} \tag{4b}$$

$$\dot{\varepsilon}_{ij}^{p} = \sum_{\alpha} \left(\dot{\varepsilon}_{ij}^{p}\right)_{\alpha} = \sum_{\alpha} \dot{\lambda}_{\alpha} \frac{\partial Q_\alpha}{\partial \sigma_{ij}} \tag{4c}$$

where $\dot{\varepsilon}_{ij}$ is the increment of strain tensor, $\dot{\sigma}_{ij}$ is the increment of stress tensor, D_{ijkl}^{e} is the fourth order elastic tensor, subscript α stands for each yield surface, $\dot{\lambda}$ is the plastic multiplier and superscripts e and p indicate elastic and plastic, respectively. Equations 4 represents the additivity postulate, Hooke's law and flow rules for each yield mechanism (Vermeer 1978, Simo et al. 1988, Hofstetter et al. 1993, Simo & Hughes 1998). The total rate of plastic strain in Equation (4c) is the summation of the rate of plastic strain calculated for all the mechanisms. Note that the constitutive model presented here is an elasto-perfect-plastic model with no hardening parameter. That is why the hardening parameter and hardening/softening rules are not included in the set of Equations 4.

For any process of loading/unloading, the Kuhn-Tucker conditions (Luenberger 1984) must be satisfied for all the mechanisms:

$$F_\alpha(\sigma_{ij}) \le 0 \quad ; \quad \dot{\lambda}_\alpha \ge 0 \quad ; \quad \dot{\lambda}_\alpha F_\alpha = 0 \tag{5}$$

The plastic potential for the Generalized Hoek-Brown yield surface has a similar function as in Equation 1 with a dilation factor m_q replacing the m_b. For the weak planes, a constant dilation angle is considered and the plastic potential function has the same form as the Coulomb criterion in Equation 2. The tension cutoffs have associated flow rules.

3.2 *Example I: Uniaxial compression tests*

As an example, Figure 2 shows the anisotropic effects induced by one and two sets of weak planes on the maximum axial strength of a rock mass sample tested in a biaxial tests configuration. The material properties for the matrix and the weak planes are listed in Table 1. Weak planes set I is oriented at angle θ_1 and set II is perpendicular to set I at angle $\theta_2 = 90° - \theta_1$. The results include the cases where only one set of the weak planes (either set I or set II) exists in the medium and the case that both sets are present. The variation of maximum axial stress with the inclination angle of the weak planes from both the analytical solution and the finite element simulations are presented in Figure 2. The analytical solutions are from a simple evaluation of failure functions for the weak planes and the matrix for different configurations of the model under uniaxial loading (Pietruszczak 2010). Similar patterns for the variation of maximum axial stress with inclination angle have been reported by many researchers both in numerical and experimental investigations (e.g. Hoek & Brown 1980, Zienkiewicz & Pande 1977).

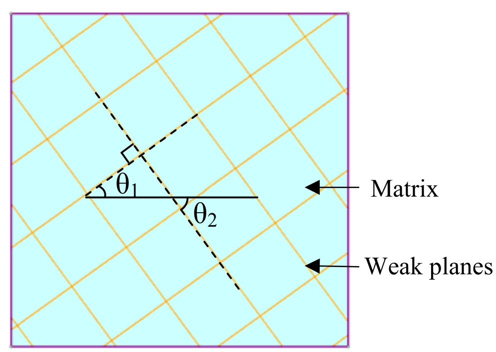

Figure 1. Typical control volume of a material with two sets of perpendicular weak planes with inclination angle θ_1 and θ_2.

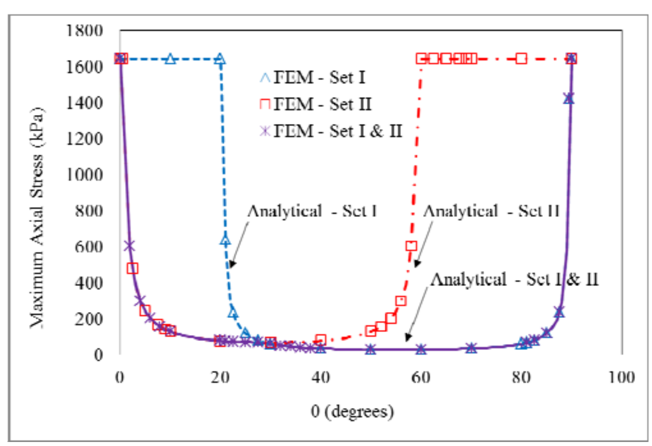

Figure 2. Variation of maximum axial stress of the rock mass sample intercepted by two sets of perpendicular weak planes.

Table 1. Properties for the matrix and weak planes

Characteristics of the matrix	Value
Unit Weight	20 kN/m^3
Elastic Modulus	50 MPa
σ_{ci}	5 MPa
m_b , m_q	3.42679
s	0.108368
a	0.500593
GSI	80
D	0
m_i	7
Weak Planes Set I	**Value**
Friction & Dilation Angle	20^O
Cohesion	10 kPa
Weak Planes Set II	**Value**
Friction & Dilation Angle	30^O
Cohesion	20 kPa

3.3 *Example II: Circular excavation*

This example presents the numerical results obtained for a circular excavation in a jointed rock mass. Two types of simulations have been performed. In the first one, the weak planes are simulated by joint networks in the finite element mesh, i.e. the joints are modeled explicitly. The second simulation takes advantage of the proposed constitutive model with embedded weak planes. The domain of the problem is a circular disk with a radius of 5m, and the circular excavation is located at the center of the disk with the radius of 1m. The simulations are plane strain and the boundary condition at the external boundary is pinned. The initial stress field is hydrostatic with a pressure equal to 100 kPa, and the body force is not included in the analysis. The material properties of the intact rock are taken from Table 1, and the weak planes have the properties of weak plane set I in that table.

In one set of simulations only one set of weak planes oriented at $\theta = 45°$ is considered, and in the second set two sets of perpendicular weak planes with $\theta_1 = 45°$ and $\theta_2 = 135°$ (see Figure 3).

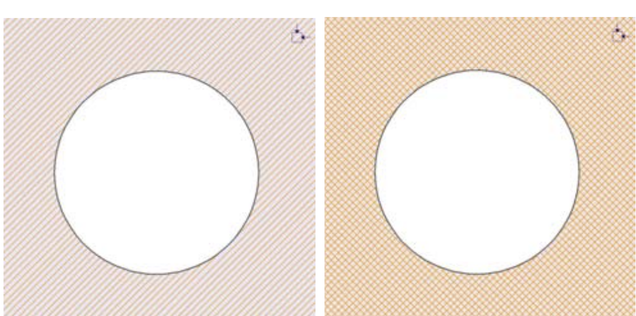

Figure 3. Circular excavation in a rock mass with one and two sets of weak planes (illustration of the explicit joint networks)

Figure 4 and 5 show the results of simulations for the case where the rock mass has only one set of weak planes with inclination angle $\theta = 45°$. Figure 4(a) shows the contours of total displacement in the domain from the simulation with the new constitutive model. Figure 4(b) shows the results obtained from the simulation that uses a joint networks. Figure 5 shows the failure pattern observed in these two simulations. The "+" symbols in Figure 5(a) are indications of failure along the weak planes at Gaussian integration points. The bold red lines in Figure 5(b) represent the slip along the explicit joints. In these simulations the plastic deformation is in the form of slips along the weak planes and no failure was observed in the intact rock.

Figures 6 and 7 present the numerical results for the case where two sets of weak planes exist at $\theta_1 = 45°$ and $\theta_2 = 135°$. Note that the properties of both sets of weak planes are the same as weak planes set I in Table 1. Figure 6 shows the contours of mean principal stress and Figure 7 illustrates the failure pattern.

Note that in these simulations since the geometry is symmetric and the field stress is constant, if the material was isotropic the results would have been symmetric as well. The asymmetry observed in the numerical results is the result of anisotropic effects induced by the weak planes.

Clearly there is a good agreement between the two approaches in modeling the weak planes in a finite element analysis.

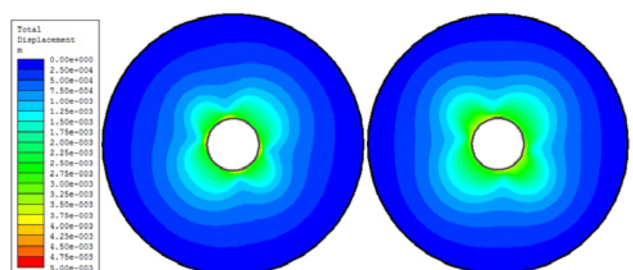

(a) (b)

Figure 4. Contours of total displacement for the case of one set of weak planes oriented at $\theta = 45°$; (a) Constitutive model with embedded weak planes and (b) joint network

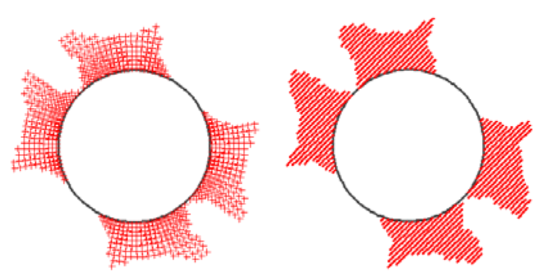

(a) (b)

Figure 5. Failure pattern around the excavation for the case of one set of weak planes oriented at $\theta = 45°$; (a) Constitutive model with embedded weak planes and (b) joint network

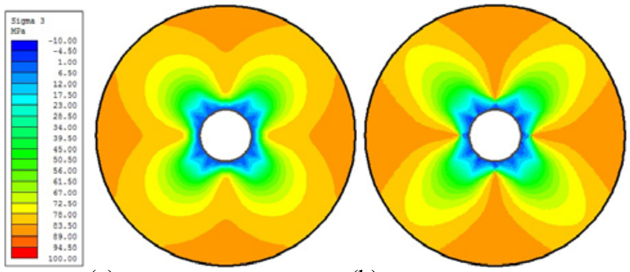

(a) (b)

Figure 6. Contours of mean principal stress for the case of two sets of weak planes oriented at $\theta_1 = 45°$ and $\theta_2 = 135°$; (a) Constitutive model with embedded weak planes and (b) joint network

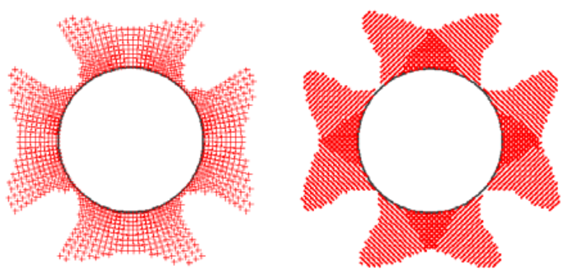

(a) (b)

Figure 7. Failure pattern around the excavation for the case of two sets of weak planes oriented at $\theta_1 = 45°$ and $\theta_2 = 135°$,; (a) Constitutive model with embedded weak planes and (b) joint network

4 SLOPE STABILTY IN JOINTED ROCK MASS

The finite element method with the shear strength reduction (SSR) method (Azami et. al. 2012, Hammah et. al. 2006, Dawson et al. 1999, Griffiths & Lane 1999) is used to evaluate the safety factor of slopes against failure. In this method, finite element analyses are used systematically to search for a strength reduction factor (SRF), i.e. the factor of safety, which brings a slope to the point of failure. Here, the SRF is applied to both the Generalized Hoek-Brown criterion for the matrix and the Coulomb criterion for the weak planes.

4.1 *SSR for the new constitutive model*

Application of SRF to the Coulomb criterion is rather straight forward. It would suffice to divide the right hand side of Equation 2 by the scalar value that is the SRF. However, for the Generalized Hoek-Brown model this task is more challenging.

There are number of approaches for applying the SRF to the Generalized Hoek-Brown model in the literature, most of which rely on some sort of a fitting procedure. In some, the Hoek-Brown criterion is locally fitted using a Mohr-Coulomb criterion based on the stress level at the material calculation point (e.g. Dawson et al 2000). In the approach proposed by Hammah et al. (2005), a new and reduced Generalized Hoek-Brown criterion is formulated based on the locally fitted Mohr-Coulomb criterion. The approach selected in this paper is based on the work of Benz et al (2008). In this approach, the yield function is modified to incorporate a SRF in its definition (see Equation 6). The simplicity and computational efficiency of this method are the reasons for this selection.

$$\sigma_1 - \sigma_3 - \frac{1}{\eta}\sigma_{ci}\left(m_b \frac{\sigma_3}{\sigma_{ci}} + s\right)^a = 0 \qquad (6)$$

In above η is a factor that is related to the SRF as follows:

$$\eta = \frac{1}{2}\left[SRF\left(2+\tilde{f}'\right)\sqrt{1+\frac{\left(SRF^{-2}-1\right)\tilde{f}'^2}{\left(2+\tilde{f}'\right)^2}} - \tilde{f}'\right] \qquad (7)$$

$$\tilde{f}' = \frac{\partial\left[\sigma_{ci}\left(m_b \frac{\sigma_3}{\sigma_{ci}} + s\right)^a\right]}{\partial \sigma_3} \qquad (8)$$

4.2 *Numerical results and discussion*

The rock mass material considered for the slope stability analysis consists of the intact material intercepted by only one set of weak planes. The material properties of the rock mass are presented in Table 1 and the properties of the weak planes corresponds to the weak planes set I in that table.

Figure 8 shows the geometry of the problem where θ is the orientation of the planes with respect to the horizontal plane and h=150m. The finite element simulations are carried out in two-dimensional plane strain configuration using 6-noded triangular elements. The external boundary of the model is constrained in both horizontal and vertical directions.

In finite element SSR simulations, θ varies from $\theta = 0°$ to $\theta = 180°$ with steps of $\Delta\theta = 5°$. On top of these, another simulation is carried out considering only the intact material with no weak planes.

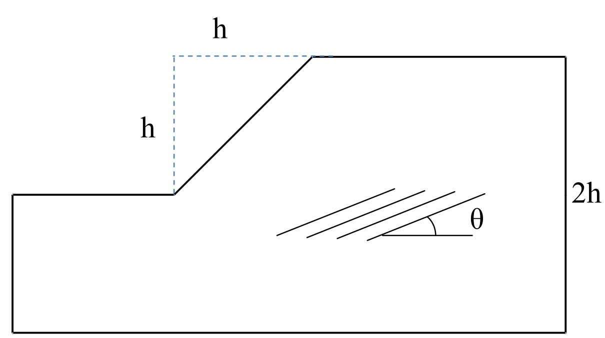

Figure 8. Geometry of the slope analyzed in this study.

Limit equilibrium analyses (Spencer 1967, Balmer 1952) were carried out using *Slide* (Rocscience Inc. 2010). The generalized anisotropic behavior was considered for the simulations where the composite material had the properties of the weak planes with orientations ranging of θ ± 2°, and the properties of the intact rock for orientations other than that range. The configuration for θ = 45° is illustrated in Figure 9. Note that in limit equilibrium analysis, for the weak planes to have any effect on the stability, they should be aligned in the direction of slip surface (Zienkiewicz & Pande 1977). Thus for θ > 90° and even close to this value, the weak planes will show no effect on the stability of slope in a typical limit equilibrium analysis. In this set of simulations, θ varies from θ = 0° to θ = 65° with steps of Δθ = 5°. Similar to the finite element simulations, an additional analysis is carried out considering only the intact material with no weak planes.

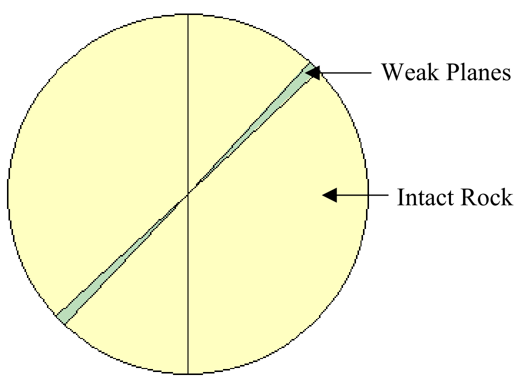

Figure 9. The composite material with generalized anisotropic strength properties used in limit equilibrium analysis (θ = 45°)

Figure 10 presents the results of a set of finite element SSR simulations. The figures show distributions of maximum shear strain (distortion) for the SRF at failure. The results presented here are for the cases of no weak planes and one set of weak planes oriented at θ equal to 0°, 15°, 35°, 50° and 55°, respectively. The slip surface predicted by the limit equilibrium analysis is also included in each figure.

The high intensity of distortion indicates the location of the slip surface. The first observation is that the shape of the failure surface is highly dependent on the orientation of weak planes. In the absence of weak planes, the slip surface has its classical circular shape (see Figure 10a). In the absence of weak planes, the finite element SSR predicts a safety factor of 2.12 for the slope, while the limit equilibrium analysis evaluates the safety factor to be 2.20. The presence of weak planes forces the failure surface to deviate from its original circular form. For θ = 0° and θ = 35°, the noncircular failure surface and the influence of weak planes is very clear.

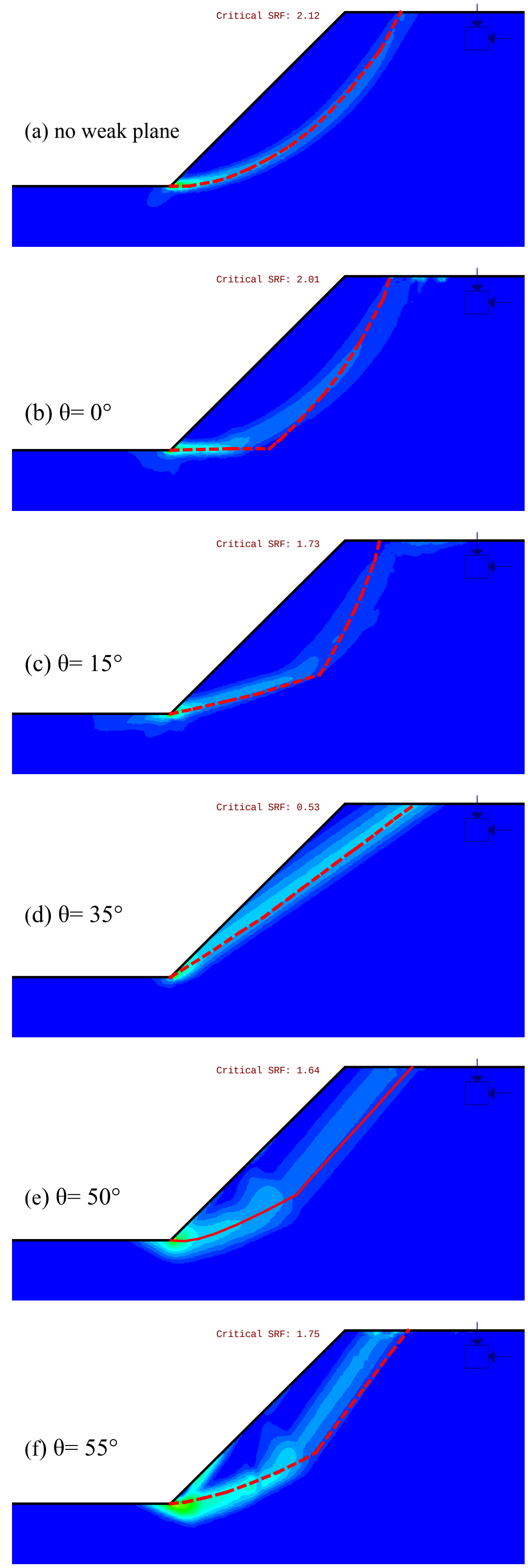

Figure 10. Numerical simulation results; the distribution of distortion in the domain obtained from finite element analyses using the constitutive model with embedded weak planes, and the slip surface predicted by limit equilibrium analysis, for the cas-

es of no weakness planes and θ equal to 0°, 15°, 35°, 50° and 55°.

The evaluated safety factors are also highly affected by the inclination angle as they vary from 2 to about 0.4. Evidently, the safety factor is higher in the absence of weak planes. Clearly by not considering the weak planes and their configuration in the slope stability simulations, the evaluation of safety factor would be far from being safe.

The variation of safety factor with the orientation of the weak planes is presented in Figure 11. There is a good agreement between the finite element SSR results with the limit equilibrium results in cases where the weak planes are aligned in the direction of the slip surface, i.e. $0° \leq \theta \leq 60°$. Based on that, it can be concluded that for other orientations, where the limit equilibrium approach cannot estimate an accurate safety factor, the finite element SSR results are valid.

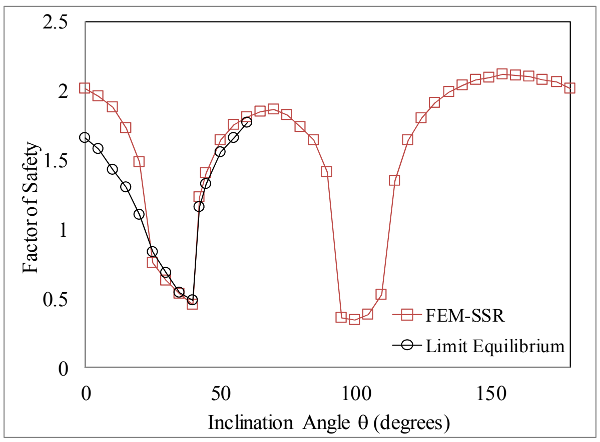

Figure 11. Variation of factor of safety with the inclination angle of weak planes.

5 CONCLUSION

The effects of strength anisotropy of geomaterials due to the presence of weak planes in the material on the stability of slopes were studied in this paper. To utilize this investigation, a constitutive model was developed based on the notion of the multi-yield-surface elasto-plastic constitutive framework. The constitutive model is composed of 4 major shear failure mechanisms, i.e. Generalized Hoek-Brown for intact material and three sets of Coulomb weak planes, and their corresponding tension cut off criteria. The multi-yield surface plasticity model was programmed as an extension to a finite element program and was used in finite element SSR simulations to calculate the safety factor of slopes in such materials. The results of finite element SSR simulations were verified by limit equilibrium analysis where possible. It was shown that the stability of slopes is highly dependent on the presence and configuration of the weak planes in the material. The shape of the possible slip surface is also influenced by the orientation of the weak planes.

6 REFERENCES

Azami A., Yacoub T. & Curran J., 2012. Effects of strength anisotropy on the stability of slopes. *65th Canadian Geotechnical Conference, CGS Geo-Manitoba*, Winnipeg, Manitoba, Canada.

Balmer, G. 1952. A general analytical solution for Mohr's envelope. *American Society for Testing and Materials*, (52): 1260-1271

Bandis, S.C., Lumsden, A.C. & Barton, N.R., 1983. Fundamentals of rock joint deformation. *International Journal of Rock Mechanics, Mining Sciences & Geomechanics Abstracts*, 20(6): 249-268.

Benz, T., Schwab, R., Kauther, R.A. & Vermeer, P.A. 2008. A Hoek–Brown criterion with intrinsic material strength factorization. *International Journal of Rock Mechanics & Mining Sciences*, 45: 210–222.

Dawson, E.M., Roth, W.H. & Drescher, A. 1999. Slope stability analysis by strength reduction, *Geotechnique*, 49(6): 835-840.

Goodman, R.E., Taylor, R.L. & Brekke, T.L., 1968. A model for the mechanics of jointed rock. *Journal of the Soil Mechanics and Foundations Division*, ASCE, 637-659.

Griffiths, D.V., & Lane, P.A. 1999. Slope stability analysis by finite elements, *Geotechnique*, 49(3): 387-403.

Hammah, R.E., Yacoub, T.E., & Curran, J.H. 2006. Investigating the performance of the shear strength reduction (SSR) method on the analysis of reinforced slopes. *In Proceedings of the 59th Canadian Geotechnical and 7th Joint IAH-CNC and CGS Groundwater Specialty Conferences – Sea to Sky Geotechnique*, Vancouver, Canada.

Hoek, E. (1983), Strength of jointed rock masses. *Geotechnique*, 33(3): 187-205.

Hoek, E. and Brown, E.T. 1980. *Underground Excavations in Rock* . London, Insiyute of Min. Metal, England.

Hoek, E., Carranza-Torres, C., Corkum, B. 2002. Hoek-Brown failure criterion—2002 edition. In: *Proceedings of the 5th North American symposium*, NARMS-TAC, Toronto.

Hofstetter, G., Simo, J.C. & Taylor, R.L. 1993. A modified cap model: closest point solution algorithm. *Computers and Structures*, 46(2): 203-214.

Luenberger, D.G. 1984. *Linear and Nonlinear Programming. Reading*, Massachusetts, Addison-Wesley.

Pietruszczak S. 2010. *Fundamentals of Plasticity in Geomechanics*. CRC Press/Balkema, The Netherlands.

Rocscience Inc. 2011, *Phase*^{2} Version 8.0 - Finite Element Analysis for Excavations and Slopes. www.rocscience.com, Toronto, Ontario, Canada.

Rocscience Inc. 2010, *Slide* Version 6.0 - 2D Limit Equilibrium Slope Stability Analysis. www.rocscience.com, Toronto, Ontario, Canada.

Simo, J.C. & Hughes T.J.R. 1998. *Computational Inelasticity*: Springer Verlag.

Simo, J.C., Kennedy, J.G. & Govindgee, S. 1988. Non-smooth multisurface plasticity and viscoplasticity, Loading/unloading conditions and numerical algorithms. *International Journal of Numerical Methods in Engineering*, 26(10): 2161-2185.

Spencer E. 1967. Method of analysis of the Stability of Embankments Assuming Parallel Inter-Slice Forces, *Geotechnique*, 17(1): 11 –26.

Vermeer P.A. 1978. A double hardening model for sand. *Geotechnique*, 28(4): 413-433.

Zienkiewicz, O.C. & Pande G.N. 1977. Time-dependent multilaminate model of rocks-A numerical study of deformation and failure of rock masses, *International Journal for Numerical and Analytical Methods in Geomechanics*, 1(3): 219–247.